Generating Coherent Phonon Waves in Narrow-Band Materials: A Twisted Bilayer Graphene Phaser

Iliya Esin, Ilya Esterlis, Eugene Demler, and Gil Refael

Phys. Rev. Lett. **130**, 147001 — Published 7 April 2023

DOI: 10.1103/PhysRevLett.130.147001

Generating coherent phonon waves in narrow-band materials: a twisted bilayer graphene phaser

Iliya Esin,[1] Ilya Esterlis,[2] Eugene Demler,[3] and Gil Refael[1]

[1] *Department of Physics and Institute for Quantum Information and Matter, California Institute of Technology, Pasadena, California 91125, USA*
[2] *Department of Physics, Harvard University, Cambridge MA 02138, USA*
[3] *Institute for Theoretical Physics, ETH Zurich, 8093 Zurich, Switzerland*

(Dated: March 21, 2023)

Twisted bilayer graphene (TBG) exhibits extremely low Fermi velocities for electrons, with the speed of sound surpassing the Fermi velocity. This regime enables the use of TBG for amplifying vibrational waves of the lattice through stimulated emission, following the same principles of operation of free-electron lasers. Our work proposes a lasing mechanism relying on the slow-electron bands to produce a coherent beam of acoustic phonons. We propose a device based on undulated electrons in TBG, which we dub the phaser. The device generates phonon beams in a terahertz (THz) frequency range, which can then be used to produce THz electromagnetic (EM) radiation. The ability to generate coherent phonons in solids breaks new ground in controlling quantum memories, probing quantum states, realizing non-equilibrium phases of matter, and designing new types of THz optical devices.

Introduction.— Controlling and manipulating phonons is a long-sought goal offering a multitude of applications in electronics, information processing, and material science [1–8], known as phononics. Recently, high-amplitude beams of phonons were employed to induce superconductivity [9–16] and to control ferroelectricity [17–21] and magnetism [22–37]. Developing reliable sources of phonons is therefore of key importance for future advances in the field of phononics. Generation of coherent phonons in solids can be achieved through pumping by intense laser and magnetic fields [38–42], or by the acoustic Cherenkov effect [43–46].

A laser of phonons (i.e., a device for amplification of sound waves by stimulated emission) can serve as an efficient source of strong coherent acoustic waves with a narrow linewidth. Such devices were realized in the low-frequency range, radio to gigahertz, in trapped ions [47–49], optical tweezers [50], nanomechanical resonators [51–56], and magnetic systems [57, 58]. A coherent amplification of terahertz (THz) phonons, yet below the threshold, was recently demonstrated in semiconductor superlattices [59], and in pump-probe experiments in SiC [60].

Here, we present a model of a device for a controlled amplification of acoustic THz phonons, based on the newly-discovered narrow-band materials, whose unique bandstructures allow coherent phonon amplification in a narrow linewidth with low losses to incoherent modes. Furthermore, acoustic phonons have a long lifetime, giving rise to a high-gain and low-loss device [61]. Although generators of coherent sound waves are often referred to as "sasers" [62], we dub our narrow-band-based device a "phaser", to highlight the phonon nature of the underlying mechanism.

Narrow-band materials such as twisted bilayer graphene (TBG) [63–65] and other moiré heterostructures [66, 67] have an electronic bandwidth controlled by the twist angle. The spectrum of the acoustic phonons of the TBG near the magic angle (where the band is flattened) is insensitive to the twist angle [68–70], resulting in a "*slow-electron*" regime where the speed of sound surpasses electronic group velocities [71], and spontaneous emission of acoustic waves is kinematically suppressed.

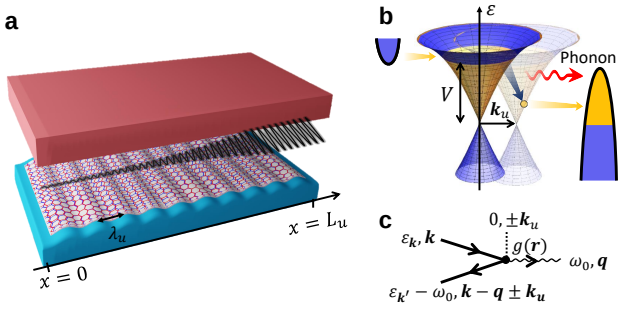

FIG. 1. **Proposed phaser device, and the key phonon-emission process. (a)** Device schematics. A layer of TBG is encapsulated between two tunneling contacts of doped semiconductors. A nano-undulator is realized by a modulated in-space uniaxial strain. Electrons produce a coherent phonon beam whose resonant frequency is controlled by the wavelength of the periodic structure, λ_u. **(b)** Band structure and Phonon-emission processes. Blue (orange) areas indicate occupied (depleted) regions in the range $\varepsilon = [0, V]$. Population inversion is imposed by the leads depicted by the two parabolas. Phonon emission resonances occur between two replicas of the bands shifted by the wavevector $\boldsymbol{k}_u$, induced by the nano-undulator. **(c)** Phonon emission Feynman diagrams. Solid lines indicate incoming and outgoing electrons, a wiggly line indicates an emitted phonon, and the dashed line indicates extra crystal momentum provided by the periodicity of the nano-undulator. In the slow-electron regime, the energy and crystal momentum can be only conserved in the presence of the momentum shift $\boldsymbol{k}_u$.

Our proposed device is based on a TBG tuned close to the magic angle and weakly spatially modulated by a periodic uniaxial strain or an array of gates (Fig. 1a). The modulation period defines the resonant phaser phonon mode. Remarkably, for lasing in the THz range, the modulation wavelength should be in the mesoscopic scale. External leads produce the needed electronic population inversion, as in semiconductor laser diodes [72].

Toy model.— Postponing a numerical analysis of the full TBG band structure, we first consider a Dirac Hamiltonian toy model, which applies to the low-energy physics of generic 2D lattices in the slow-electron regime:

$$\mathcal{H}_{\rm D}(\boldsymbol{k}) = \hbar v_{\rm e} \boldsymbol{k}\cdot\boldsymbol{\sigma}. \tag{1}$$

$\boldsymbol{k} = (k_x, k_y)$ is the in-plane crystal momentum, $\boldsymbol{\sigma} = (\sigma^x, \sigma^y)$ a vector of pseudo-spin Pauli matrices, and $v_{\rm e} > 0$ the electronic velocity. Eq. (1) is diagonalized by the Bloch states $\frac{e^{i\boldsymbol{r}\cdot\boldsymbol{k}}}{\sqrt{\mathcal{A}}}|\psi_{\boldsymbol{k}\alpha}(\boldsymbol{r})\rangle$, corresponding to the eigenvalues $\varepsilon_\alpha(\boldsymbol{k}) = \alpha\hbar v_e|\boldsymbol{k}|$, where $\alpha = \pm$, $|\psi_{\boldsymbol{k}\alpha}(\boldsymbol{r})\rangle$ is periodic in the unit cell, and $\mathcal{A}$ is the area of the system. The eigenstates are created by the operators $\hat{c}^\dagger_{\boldsymbol{k}\alpha}$. In the toy model, we assume no spin or pseudospin degrees other than $\boldsymbol{\sigma}$ (additional degrees of freedom such as valley, spin, and layer indices of the TBG would not qualitatively change the effect).

Concentrating on the $v_{\rm e} < c_{\rm ph}$ regime, with $c_{\rm ph}$ the speed of sound, assumed uniform and isotropic. Sound waves are described by the lattice displacement operator $\hat{\boldsymbol{u}}(\boldsymbol{r},t) = (\hat{u}_x, \hat{u}_y)$[73], which can be expanded in the eigenmodes $\hat{\boldsymbol{u}}(\boldsymbol{r},t) = \frac{1}{\sqrt{\mathcal{A}}}\sum_{\boldsymbol{q}} e^{i\boldsymbol{q}\cdot\boldsymbol{r}-i\omega_l(\boldsymbol{q})t}\boldsymbol{c}_l(\boldsymbol{q})\tilde{u}_l(\boldsymbol{q})$. Here, $\boldsymbol{r} = (x,y)$, and $\boldsymbol{c}_l(\boldsymbol{q})$ is the unit vector denoting the direction of the displacement in the mode l and crystal momentum $\boldsymbol{q}$. Focusing on the lowest energy acoustic mode with $l = 0$, we assume a dispersion $\omega_0(\boldsymbol{q}) = c_{\rm ph}|\boldsymbol{q}|$, and coupling to electrons

$$\hat{\mathcal{H}}_{\rm ep} = \int d^2\boldsymbol{r} g(\boldsymbol{r})\hat{\mathcal{O}}_{ij}(\boldsymbol{r})\partial_i\hat{u}_j(\boldsymbol{r}). \tag{2}$$

Here, $\hat{\mathcal{O}}_{ij}(\boldsymbol{r})$ is a local electronic operator with $i,j = \{x,y\}$, and $g(\boldsymbol{r})$ is the coupling strength with a position dependence explicitly specified below.

Two external leads produce an electronic population inversion. An electron-doped semiconductor contact has a chemical potential set at $\varepsilon = \varepsilon_{\rm top}$, corresponding to the top of the upper band of the TBG [denoted by $\alpha = +$, see below Eq. (1)], and a hole-doped semiconductor contact is set to the charge neutrality point of the TBG, $\varepsilon = 0$. We assume that tunneling between the system and the leads is faster than the electronic decay rates due to relaxation and phonon emission [74]. Assuming this and *zero-temperature* leads, the electronic occupation probability $f_{\alpha\boldsymbol{k}} = \langle\hat{c}^\dagger_{\alpha\boldsymbol{k}}\hat{c}_{\alpha\boldsymbol{k}}\rangle$ is approximated by $f_{\alpha\boldsymbol{k}} = 0$ for $0 < \varepsilon_\alpha(\boldsymbol{k}) < V$, and $f_{\alpha\boldsymbol{k}} = 1$ otherwise, imposing population inversion in the upper band (Fig. 1b).

When the electron-phonon (e-ph) coupling is *spatially uniform*, the electronic population inversion is virtually decoupled from the phonons. Indeed, the "slow-electron" regime renders conserving energy and crystal momentum simultaneously impossible within a single-phonon emission. As a result, the incoherent phonon background field created by the inverted electronic state is suppressed. This e-ph decoupling is crucial for lasing. Yet the electrons should be coupled to at least one phonon mode, to generate a coherent beam.

Inspired by free-electron lasers [75–78], emission into a selected mode can be induced by spatially modulated e-ph coupling, $g(\boldsymbol{r})$. Below, we let $g(\boldsymbol{r})$ depend on the $x = \boldsymbol{r}\cdot\hat{\boldsymbol{x}}$ coordinate, with a wavelength $\lambda_u = 2\pi/k_u$, $g(\boldsymbol{r}) = g_0 + 2g_1\cos(k_u x)$ (see Fig. 1a). We denote the region of the system where $g_1 \neq 0$, a *nano-undulator*, by analogy with the FEL magnetic undulator, and discuss its physical realization below.

In the nano-undulator, phonon emission processes obey $\boldsymbol{k}' - \boldsymbol{k} = \boldsymbol{q} + nk_u\hat{\boldsymbol{x}}$, where $\boldsymbol{k}$, $\boldsymbol{k}'$ are respectively the electronic crystal momenta before and after emitting a phonon with momentum $\boldsymbol{q}$, and $n = \{-1, 0, 1\}$ [Fig. 1c]. The momentum shift arises from the Fourier expansion of $g(\boldsymbol{r})$ in Eq. (2): $g(\boldsymbol{r}) = \sum_n g_n e^{ink_u x}$, where $g_1 = g_{-1}$. Energy conservation, however, remains $\varepsilon_+(\boldsymbol{k}') - \varepsilon_+(\boldsymbol{k}) = \hbar\omega_0(\boldsymbol{q})$. Energy and crystal momentum conservation is satisfied by two resonant $\hat{\boldsymbol{x}}$-direction phonon modes with frequencies

$$\omega_{R\pm} = \frac{c_{\rm ph}k_u}{(c_{\rm ph}/v_{\rm e}) \pm 1}. \tag{3}$$

Thus, the resonant frequency of the phaser is controlled by tuning the nano-undulator wavevector, k_u.

Gain estimation starts with considering a coherent sound wave incident at $x = 0$ with amplitude $\boldsymbol{u}_0$ and frequency ω, propagating along $+\hat{\boldsymbol{x}}$ (generated, i.e., by a seed or by spontaneous emission processes), Fig. 1a. Sound amplification in the nano-undulator is captured by an exponential factor with the gain coefficient γ_ω [72]

$$\boldsymbol{u}_\omega(\boldsymbol{r},t) = \boldsymbol{u}_0 e^{\gamma_\omega x}e^{i(qx-\omega t)}, \tag{4}$$

where $q = \omega/c_{\rm ph}$. Such a sound wave, after passing the nano-undulator, carries a period-averaged power density

$$\mathcal{P}_{\rm s}(\omega) = \frac{1}{2a^2L_u}c_{\rm ph}M\omega^2|\boldsymbol{u}_0|^2(e^{2\gamma_\omega L_u} - 1), \tag{5}$$

where L_u is the nano-undulator length, M is the atomic mass of the underlying material, and a is lattice constant.

In the low-gain limit, the period-averaged power density emitted by the electrons stimulated by the field $\boldsymbol{u}_\omega$, can be found using Fermi's golden rule [79],

$$\mathcal{P}_{\rm e}(\omega) = \frac{2\pi\omega}{\mathcal{A}}\sum_{\alpha\alpha',\boldsymbol{k}\boldsymbol{k}'} f_{\alpha\boldsymbol{k}}[\mathcal{M}^{\alpha\alpha'}_{\boldsymbol{k}\boldsymbol{k}'}\delta(\varepsilon_\alpha(\boldsymbol{k}) - \varepsilon_{\alpha'}(\boldsymbol{k}') - \hbar\omega) - \mathcal{M}^{\alpha\alpha'}_{\boldsymbol{k}'\boldsymbol{k}}\delta(\varepsilon_\alpha(\boldsymbol{k}) - \varepsilon_{\alpha'}(\boldsymbol{k}') + \hbar\omega)]. \tag{6}$$

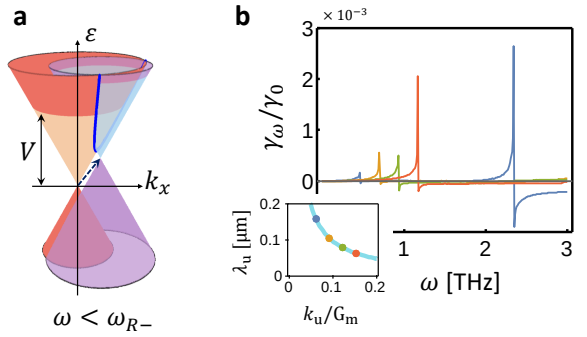

FIG. 2. **The gain in the toy model.** (**a**) Dirac dispersion of the electrons as in Eq. (1) and a copy shifted by the energy ω and crystal momentum $q + k_u$ in the $\hat{\boldsymbol{x}}$ direction (dashed arrow). The phonon emission rate is proportional to the intersection area of the two Dirac dispersions [Eq. (6)], indicated by the blue line. (**b**) The gain of the device normalized by γ_0 [see Eq. (8)] as a function of the phonon frequency calculated in the toy model, for four values of k_u. The values of k_u and the corresponding wavelengths $\lambda_u = 2\pi/k_u$ are indicated in the inset. The gain exhibits resonance peaks at the frequencies given by Eq. (3).

Here, $(\alpha, \boldsymbol{k})$ and $(\alpha', \boldsymbol{k}')$ respectively denote the electronic band and crystal momentum before and after the interaction with the acoustic wave and $\mathcal{M}^{\alpha\alpha'}_{\boldsymbol{k}\boldsymbol{k}'} = |\mathcal{A}^{-1}\int d^2\boldsymbol{r} e^{i\boldsymbol{r}(\boldsymbol{k}-\boldsymbol{k}')}\langle\psi_{\alpha\boldsymbol{k}}(\boldsymbol{r})|\hat{\mathcal{H}}_{\rm ep}|\psi_{\alpha'\boldsymbol{k}'}(\boldsymbol{r})\rangle|^2$, where the integration is over the nano-undulator area. [For coherent phonon generation in a more generic case one can use e-ph instabilities as outlined in the Supp. Mat.]

Since the sound wave is coherent, the acoustic field operator in $\hat{\mathcal{H}}_{\rm ep}$ can be replaced [Eq. (2)] by its expectation value $\langle\hat{\boldsymbol{u}}\rangle \approx \boldsymbol{u}_\omega$, given in Eq. (4). Then we obtain $\mathcal{M}^{\alpha\alpha'}_{\boldsymbol{k}\boldsymbol{k}'} = q^2|\boldsymbol{u}_0|^2\sum_n|\frac{g_n}{\mathcal{A}}|^2|\int d^2\boldsymbol{r} e^{\gamma_\omega x}e^{i\boldsymbol{r}(\boldsymbol{k}-\boldsymbol{k}'-(q+nk_u)\hat{\boldsymbol{x}})}\langle\hat{\mathcal{O}}\rangle^{\alpha\boldsymbol{k}}_{\alpha'\boldsymbol{k}'}|^2$, where $\langle\hat{\mathcal{O}}\rangle^{\alpha\boldsymbol{k}}_{\alpha'\boldsymbol{k}'} = \int d^2\boldsymbol{r}\langle\psi_{\alpha\boldsymbol{k}}|\hat{\mathcal{O}}_{xi}(\boldsymbol{r})c_i|\psi_{\alpha'\boldsymbol{k}'}\rangle$, and c_i is the i-th component of the unit vector along $\boldsymbol{u}_0$.

Assuming $\langle\mathcal{O}\rangle$ depends weakly on momentum, and taking a small gain limit $\gamma_\omega \to 0$, $\mathcal{M}^{\alpha\alpha'}_{\boldsymbol{k}\boldsymbol{k}'}$ is non-zero only when $|\boldsymbol{k} - \boldsymbol{k}' - (q + nk_u)\hat{\boldsymbol{x}}|^2 < (2\pi)^2/\mathcal{A}$. In the thermodynamic limit ($\mathcal{A} \to \infty$), the values of $\boldsymbol{k}$ contributing to the sum in the expression for $\mathcal{P}_{\rm e}(\omega)$ in Eq. (6), lie near the intersection line of two cones described by $\varepsilon_\alpha(\boldsymbol{k})$ and $\varepsilon_{\alpha'}(\boldsymbol{k}') + \hbar\omega$, where $\boldsymbol{k}' = \boldsymbol{k} + (q + nk_u)\hat{\boldsymbol{x}}$, and $f_{\alpha\boldsymbol{k}} \neq f_{\alpha'\boldsymbol{k}'}$ (Fig. 2a). The largest value of $\mathcal{P}_{\rm e}(\omega)$ is obtained for $\omega \approx \omega_{R,n}$, where $n = \pm$ [see Eq. (3)], where the two cones are tangent. The area in the momentum space where the two cones are nearly tangential diverges as $\delta\omega_n^{-\frac{1}{2}}$, with $\delta\omega_n = \omega_{R,n} - \omega$, as ω approaches $\omega_{R,n}$ from below, giving rise to a resonance peak in $\mathcal{P}_{\rm e}(\omega)$. For $\omega > \omega_{R,n}$ the intersection line of the cone with $\alpha = +$ and the cone with $\alpha' = -$, contributes to a negative peak corresponding to the absorption of phonons.

The gain γ_ω is found by setting $\mathcal{P}_{\rm s}(\omega) = \mathcal{P}_{\rm e}(\omega)$ and using [Eqs. (5) and (6)] for $\mathcal{P}_{\rm s}(\omega)$ and $\mathcal{P}_{\rm e}(\omega)$ as a function of γ_ω. In the small gain limit ($\gamma_\omega \to 0$),

$$\gamma_\omega = \mathcal{P}^0_{\rm e}(\omega)a^2/(c_{\rm ph}M\omega^2|\boldsymbol{u}_0|^2), \tag{7}$$

where $\mathcal{P}^0_{\rm e}(\omega) = \mathcal{P}_{\rm e}(\omega)|_{\gamma_\omega=0}$. Estimating Eq. (6) in the limit $0 < \delta\omega_n \ll \omega_{R,n}$ and $V \gg \hbar\omega_{R,n}$ [79] , we find

$$\gamma_\omega = \gamma_0\sum_{n=\pm}\hbar\omega_{R,n}\sqrt{2\omega_{R,n}/\delta\omega_n}\mathcal{N}_D(V)a^2, \tag{8}$$

where $\gamma_0 = g_1^2\langle\mathcal{O}\rangle^2/(\hbar c_{\rm ph}^3 M)$ and $\mathcal{N}_{\rm D}(\varepsilon) = \varepsilon/(2\pi\hbar^2 v_{\rm e}^2)$ is the DOS of the Dirac dispersion. Fig. 2b shows γ_ω vs. ω for several k_u values shown in the inset.

Analysis of phaser realizations in TBG.— The TBG consists of two graphene monolayers twisted by a relative angle θ, giving rise to a moiré super lattice with period [80] $a_{\rm m} = a/(2\sin(\theta/2))$. Small twist angles yield a dispersion near charge neutrality with narrow bands, approximated by Eq. (1) for two spin and two valley quantum numbers [63, 81]. Let us focus on $\theta = 1.4°$, where we find $v_{\rm e} \approx 2\times10^6$ cm/sec, which is below the speed of sound, approximated by $c_{\rm ph} = 3\times10^6$ cm/sec.

We consider two alternatives for the spatial modulation of the e-ph coupling needed for the nano-undulator [see Eq. (2)] [82]. The first realization uses a spatially modulated uniaxial strain (see Fig. 1a), induced by placing the TBG on a periodic nanostructure or by applying temperature gradients [83–87]. Weak periodic strain modulates the graphene lattice, and thus also the e-ph coupling [69, 88]. For a strain, $\epsilon_0\cos(k_u x)$, the spatially-modulated part of the e-ph coupling in each monolayer can be expressed by Eq. (2) with $g_1 = \frac{\sqrt{3}}{4a}\hbar v_F\beta\epsilon_0$, and $\hat{\mathcal{O}}_{ij}(\boldsymbol{r}) = (\hat{c}^\dagger_{\boldsymbol{r},A}\hat{c}_{\boldsymbol{r},B} + \hat{c}^\dagger_{\boldsymbol{r},B}\hat{c}_{\boldsymbol{r},A})(\delta_{i,x}\delta_{j,x} - \delta_{i,y}\delta_{j,y})$, where $\hat{c}^\dagger_{\boldsymbol{r},A/B}$ creates an electron in the sublattice A or B of the graphene monolayer at the $\boldsymbol{r}$ unit cell [79]. For $\epsilon_0 \approx 5\%$ strain, we estimate $g_1 \approx 0.15$ eV, corresponding to $\gamma_0 \approx 0.02\,\mu m^{-1}$.

The second realization uses a periodic array of metallic gates at distance d from the TBG. The gates change the e-ph coupling by affecting the Coulomb screening between the electronic charge density and the lattice ions [89–95]. We approximate the renormalized coupling of a phonon with momentum q by $g(\boldsymbol{r}) = D_0 q/[q + q_{\rm TF}(1 - e^{-2qd(\boldsymbol{r})})]$, where $d(\boldsymbol{r})$ is the distance from the gates, which toggles between $d(\boldsymbol{r}) \approx d$ above a gate and $d(\boldsymbol{r}) \to \infty$ not above a gate, $q_{\rm TF}$ is the Thomas Fermi wavevector and D_0 the bare e-ph coupling. To approximate the e-ph coupling by Eq. (2), in the limit $q_{\rm TF} \gg q, 1/d$, we estimate $g_1 \approx \frac{1}{4}\frac{D_0}{1+2q_{\rm TF}d}$ and $\hat{\mathcal{O}}_{ij}(\boldsymbol{r}) \sim \hat{\rho}(\boldsymbol{r})\delta_{ij}$, where $\hat{\rho}(\boldsymbol{r}) = \hat{c}^\dagger_{\boldsymbol{r},A}\hat{c}_{\boldsymbol{r},A} + \hat{c}^\dagger_{\boldsymbol{r},B}\hat{c}_{\boldsymbol{r},B}$ measures the density. For $q_{\rm TF}d \approx 3$ [96] and $D_0 = 50$ eV, we estimate $g_1 \approx 1.8$ eV, corresponding to $\gamma_0 \approx 3\,\mu m^{-1}$.

Numerical analysis of the gain.— We simulated the continuum TBG model [63, 81] in order to verify that the full bandstructure of the TBG exhibits resonance

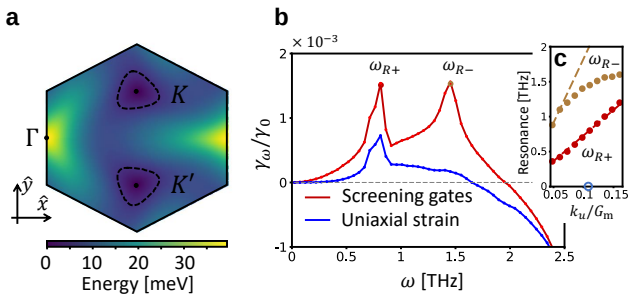

FIG. 3. **Numerical analysis of the phaser based on the TBG. (a)** The band structure of the upper band of the TBG near the charge neutrality point for a single valley, shown on a mini Brillouin zone centered around the Dirac points, K and K'. Curves around K and K' points indicate the equipotentials $\varepsilon = 6\,\mathrm{meV}$. **(b)** The gain calculated by Eqs. (6) and (7) for the wavefunctions of the TBG for the uniaxial-strain nano-undulator as well as for the array of screening gates nano-undulator, for the wavevector $k_u \approx 0.11 G_\mathrm{m}$ indicated by a circle on the x-axis in panel c. **(c)** The frequency of the resonant peaks of the gain as a function of k_u. Dashed lines are the resonances predicted by the toy model [Eq. (3)].

phonon-emission peaks, as predicted by the toy model, and compare their frequencies to Eq. (3). Fig. 3a shows the spectrum of the upper band of the TBG in a single valley in the mini-Brillouin zone centered around the Dirac points [c.f., supp. mat.]. The contours near the K and K' points are the equipotentials $\varepsilon = V$.

We evaluated the gain in the full TBG model using Eq. (7), estimating $\mathcal{P}_\mathrm{e}(\omega)$ by Eq. (6) in the two aforementioned nano-undulator realizations. Fig. 3b shows the resulting gain vs. the frequency for $k_u \approx 0.11 G_m$, where $G_m = 2\pi/a_m$, for the two nano-undulator options. Both curves exhibit a peak near $\omega \approx 0.8\,\mathrm{THz}$, corresponding to the analytical estimate of ω_{R+} [defined in Eq. (3)]. The screening gates option exhibits an additional peak near $\omega \approx 1.5\,\mathrm{THz}$, not present for the uniaxial strain option. This is due to the selection rules, which suppress transitions for large phonon frequencies.

Fig. 3c shows the frequencies of the two peaks of the screening-gates nano-undulator gain vs. k_u. Dashed lines are the prediction from $\omega_{R\pm}$ (Eq. 3). The curve of the low-frequency peak roughly coincides with the analytical curve corresponding to ω_{R+} vs. k_u with $v_\mathrm{e} = 2\times10^6\,\mathrm{cm/sec}$ [see Eq. (3)]. The position of the second peak does not show a linear dependence on k_u, as predicted by Eq. (3), due to deviations of the TBG band structure from the linear dispersion [Eq. (1)] for high phonon energies. We can fit its resonance frequency at $k_u/G_\mathrm{m} = 0.05$, by ω_{R-} with $v_\mathrm{e} = 1.5\times10^6\,\mathrm{cm/sec}$.

Lasing threshold is achieved when the gain exceeds the loss. The loss of phonons is mostly due to e-ph, ph-ph, and impurity scattering. The lifetime of acoustic phonons in clean graphene can reach $\tau_\mathrm{ph} \approx 0.3\,\mu\mathrm{sec}$, for long-wavelength phonons [97], which results in $\gamma_\mathrm{loss} = (\tau_\mathrm{ph} c_\mathrm{ph})^{-1} \approx 2\times10^{-4}\,\mu\mathrm{m}^{-1}$. This value is below the gain of the system, estimated at a frequency slightly above the resonance peak. To have a sufficient gain, the system can be placed in an acoustic cavity, e.g., as in Ref. 98. The phonon-loss in a cavity is given by $\gamma_\mathrm{cavity} = -\log(R_1R_2)/(2L_u)$, where R_1 and R_2 are the reflectivities of the two mirrors. For $R_1R_2 = 0.97$ and $L_u \approx 5\,\mu\mathrm{m}$, we obtain $\gamma_\mathrm{cavity} \approx 0.001\,\mu\mathrm{m}^{-1}$. This results in a phonon Q-factor of the cavity being $Q \sim 10^5$.

Discussion.— In this manuscript, we presented a model of a phonon laser device based on the "narrow-band" regime, dubbed a phaser. The phaser generates coherent phonon beams in the THz range. We proposed and analyzed two realizations of the phaser in near-magic-angle TBG, with a spatially modulated uniaxial strain or an array of screening gates [see Fig. 1a]. The periodicity of the structure determines the device's resonant frequency.

What could a THz phaser be used for? The phaser uniquely allows driving the TBG into a non-equilibrium regime through moiré Floquet engineering [99, 100], extending the driving sources to THz frequencies and finite momenta [101]. THz phonon sources can be used to probe low-energy excitations in solids [102, 103] in a new regime of surface acoustic waves. An electronic generator of coherent phononic beams on-demand has multiple technological applications such as superfast manipulation of magnetic memories [32, 104] and controlling ferroelectricity [17–21].

Furthermore, a phaser could generate THz EM radiation. The implied large amplitude lattice oscillations are coupled to plasmon modes both electrically and through the e-ph coupling. The resulting charged modes generate a THz EM field evanescent in the direction perpendicular to the TBG plane. The electric field amplitude near the surface is roughly [79] $|\vec{E}| = 2\sqrt{2}\pi e\rho_0\lambda q^2|\langle\hat{\boldsymbol{u}}\rangle|$. Here, λq is the relative charge fluctuation which we estimate as $\lambda q \approx 2\times10^{-2}$, and ρ_0 is the electronic density taken as $\rho_0 \approx 1/a_\mathrm{m}^2$. Assuming that the phaser in the saturation regime creates lattice waves of the order of $|\langle\hat{\boldsymbol{u}}\rangle| \approx 0.1a$, we estimate, $|\vec{E}| \approx 30\,\mathrm{kV/m}$. Such an electric field can be detected by placing a dipole antenna near the surface of the TBG. An oscillating evanescent electric field can be transformed into THz EM radiation, through a meta-material structure.

Our analysis focused on the single-particle electronic bands of the TBG. In the presence of the e-e interactions, the Fermi velocity may be renormalized, yet the slow-electron regime can be still achieved [105]. Furthermore, the Dirac dispersion near charge neutrality is protected by the $C_2\mathcal{T}$ symmetry (two-fold rotation times time-reversal) and will be preserved unless it is spontaneously broken [106–109]. Operating at temperatures near 30K, but below the temperatures of THz resonant phonons, is expected to prevent the formation of a symmetry-broken

phase. This elevated temperature allows for efficient operation while avoiding the formation of phases that may interfere with the proper functioning of the system.

The toy model of the phaser [Eq. (1)] can be realized in other experimental platforms. A "slow-band" regime can be realized, e.g., in cold atoms, using Bose-Fermi mixtures [110, 111]. The energy scales of cold atom setups, however, are a few orders of magnitude smaller than in solids, giving rise to a different range of resonant frequencies.

We thank Kenneth Burch, Jerome Faist, Mohammad Hafezi, Atac Imamoglu, Cyprian Lewandowski, Marios Michael, Leo Radzihovsky, and Christopher Yang for valuable discussions. G. Refael and I. Esin are grateful for support from the Simons Foundation and the Institute of Quantum Information and Matter, as well as support from the NSF DMR grant number 1839271. E. Demler and I. Esterlis acknowledge support from the ARO grant "Control of Many-Body States Using Strong Coherent Light-Matter Coupling in Terahertz Cavities". This work is supported by ARO MURI Grant No. W911NF-16-1-0361, and was performed in part at Aspen Center for Physics, which is supported by National Science Foundation grant PHY-1607611.

[1] M. Först, C. Manzoni, S. Kaiser, Y. Tomioka, Y. Tokura, R. Merlin, and A. Cavalleri, "Nonlinear phononics as an ultrafast route to lattice control," Nat. Phys. **7**, 854–856 (2011).

[2] Nianbei Li, Jie Ren, Lei Wang, Gang Zhang, Peter Hänggi, and Baowen Li, "Colloquium: Phononics: Manipulating heat flow with electronic analogs and beyond," Rev. Mod. Phys. **84**, 1045–1066 (2012).

[3] Alexander A. Balandin and Denis L. Nika, "Phononics in low-dimensional materials," Mater. Today **15**, 266–275 (2012).

[4] Martin Maldovan, "Sound and heat revolutions in phononics," Nature **503**, 209–217 (2013).

[5] Alexander A. Balandin, "Phononics of Graphene and Related Materials," ACS Nano **14**, 5170–5178 (2020).

[6] Alaska Subedi, Andrea Cavalleri, and Antoine Georges, "Theory of nonlinear phononics for coherent light control of solids," Phys. Rev. B **89**, 220301 (2014).

[7] Roman Mankowsky, Michael Först, and Andrea Cavalleri, "Non-equilibrium control of complex solids by nonlinear phononics," Reports Prog. Phys. **79**, 064503 (2016).

[8] D. M. Juraschek, M. Fechner, and N. A. Spaldin, "Ultrafast Structure Switching through Nonlinear Phononics," Phys. Rev. Lett. **118**, 054101 (2017).

[9] R. Mankowsky, A. Subedi, M. Först, S. O. Mariager, M. Chollet, H. T. Lemke, J. S. Robinson, J. M. Glownia, M. P. Minitti, A. Frano, M. Fechner, N. A. Spaldin, T. Loew, B. Keimer, A. Georges, and A. Cavalleri, "Nonlinear lattice dynamics as a basis for enhanced superconductivity in YBa2Cu3O6.5," Nature **516**, 71–73 (2014).

[10] M. Mitrano, A. Cantaluppi, D. Nicoletti, S. Kaiser, A. Perucchi, S. Lupi, P. Di Pietro, D. Pontiroli, M. Riccò, S. R. Clark, D. Jaksch, and A. Cavalleri, "Possible light-induced superconductivity in K3C60 at high temperature," Nature **530**, 461–464 (2016).

[11] Michael Knap, Mehrtash Babadi, Gil Refael, Ivar Martin, and Eugene Demler, "Dynamical Cooper pairing in nonequilibrium electron-phonon systems," Phys. Rev. B **94**, 214504 (2016).

[12] Andreas Komnik and Michael Thorwart, "BCS theory of driven superconductivity," Eur. Phys. J. B **89**, 1–5 (2016).

[13] Mehrtash Babadi, Michael Knap, Ivar Martin, Gil Refael, and Eugene Demler, "Theory of parametrically amplified electron-phonon superconductivity," Phys. Rev. B **96**, 014512 (2017).

[14] Dante M. Kennes, Eli Y. Wilner, David R. Reichman, and Andrew J. Millis, "Transient superconductivity from electronic squeezing of optically pumped phonons," Nat. Phys. **13**, 479–483 (2017).

[15] A. Cantaluppi, M. Buzzi, G. Jotzu, D. Nicoletti, M. Mitrano, D. Pontiroli, M. Riccò, A. Perucchi, P. Di Pietro, and A. Cavalleri, "Pressure tuning of light-induced superconductivity in K3C60," Nat. Phys. **14**, 837–841 (2018).

[16] B. Liu, M. Först, M. Fechner, D. Nicoletti, J. Porras, T. Loew, B. Keimer, and A. Cavalleri, "Pump frequency resonances for light-induced incipient superconductivity in YBa2Cu3 O6.5," Phys. Rev. X **10**, 011053 (2020).

[17] R. Mankowsky, A. Von Hoegen, M. Först, and A. Cavalleri, "Ultrafast Reversal of the Ferroelectric Polarization," Phys. Rev. Lett. **118**, 197601 (2017).

[18] T. F. Nova, A. S. Disa, M. Fechner, and A. Cavalleri, "Metastable ferroelectricity in optically strained SrTiO3," Science **364**, 1075–1079 (2019).

[19] Xian Li, Tian Qiu, Jiahao Zhang, Edoardo Baldini, Jian Lu, Andrew M. Rappe, and Keith A. Nelson, "Terahertz fieldinduced ferroelectricity in quantum paraelectric SrTiO3," Science **364**, 1079–1082 (2019).

[20] Dongbin Shin, Shunsuke A. Sato, Hannes Hübener, Umberto De Giovannini, Noejung Park, and Angel Rubio, "Dynamical amplification of electric polarization through nonlinear phononics in 2D SnTe," npj Comput. Mater. **6**, 1–8 (2020).

[21] Veniamin A. Abalmasov, "Ultrafast reversal of the ferroelectric polarization by a midinfrared pulse," Phys. Rev. B **101**, 014102 (2020).

[22] T. F. Nova, A. Cartella, A. Cantaluppi, M. Först, D. Bossini, R. V. Mikhaylovskiy, A. V. Kimel, R. Merlin, and A. Cavalleri, "An effective magnetic field from optically driven phonons," Nat. Phys. **13**, 132–136 (2016).

[23] Dominik M. Juraschek, Michael Fechner, Alexander V. Balatsky, and Nicola A. Spaldin, "Dynamical multiferroicity," Phys. Rev. Mater. **1**, 014401 (2017).

[24] Dongbin Shin, Hannes Hübener, Umberto De Giovannini, Hosub Jin, Angel Rubio, and Noejung Park, "Phonon-driven spin-Floquet magneto-valleytronics in MoS2," Nat. Commun. **9**, 1–8 (2018).

[25] Paolo G. Radaelli, "Breaking symmetry with light: Ultrafast ferroelectricity and magnetism from three-phonon coupling," Phys. Rev. B **97**, 085145 (2018).

[26] Sebastian F. Maehrlein, Ilie Radu, Pablo Maldon-

ado, Alexander Paarmann, Michael Gensch, Alexandra M. Kalashnikova, Roman V. Pisarev, Martin Wolf, Peter M. Oppeneer, Joseph Barker, and Tobias Kampfrath, "Dissecting spin-phonon equilibration in ferrimagnetic insulators by ultrafast lattice excitation," Sci. Adv. **4** (2018).

[27] Mingqiang Gu and James M. Rondinelli, "Nonlinear phononic control and emergent magnetism in Mott insulating titanates," Phys. Rev. B **98**, 024102 (2018).

[28] Guru Khalsa and Nicole A. Benedek, "Ultrafast optically induced ferromagnetic/anti-ferromagnetic phase transition in GdTiO3 from first principles," npj Quantum Mater. **3**, 1–8 (2018).

[29] M. Fechner, A. Sukhov, L. Chotorlishvili, C. Kenel, J. Berakdar, and N. A. Spaldin, "Magnetophononics: Ultrafast spin control through the lattice," Phys. Rev. Mater. **2**, 064401 (2018).

[30] Dominik M. Juraschek and Nicola A. Spaldin, "Orbital magnetic moments of phonons," Phys. Rev. Mater. **3**, 064405 (2019).

[31] Ankit S. Disa, Michael Fechner, Tobia F. Nova, Biaolong Liu, Michael Först, Dharmalingam Prabhakaran, Paolo G. Radaelli, and Andrea Cavalleri, "Polarizing an antiferromagnet by optical engineering of the crystal field," Nat. Phys. **16**, 937–941 (2020).

[32] Dominik M. Juraschek and Prineha Narang, "Shaken not strained," Nat. Phys. **16**, 900–901 (2020).

[33] M. Rodriguez-Vega, Ze Xun Lin, A. Leonardo, A. Ernst, G. Chaudhary, M. G. Vergniory, and Gregory A. Fiete, "Phonon-mediated dimensional crossover in bilayer Cr I3," Phys. Rev. B **102**, 081117 (2020).

[34] Dominik M. Juraschek, Prineha Narang, and Nicola A. Spaldin, "Phono-magnetic analogs to opto-magnetic effects," Phys. Rev. Res. **2**, 043035 (2020).

[35] Dominik M. Juraschek, Derek S. Wang, and Prineha Narang, "Sum-frequency excitation of coherent magnons," Phys. Rev. B **103**, 094407 (2021).

[36] A. Stupakiewicz, C. S. Davies, K. Szerenos, D. Afanasiev, K. S. Rabinovich, A. V. Boris, A. Caviglia, A. V. Kimel, and A. Kirilyuk, "Ultrafast phononic switching of magnetization," Nat. Phys. **17**, 489–492 (2021).

[37] D. Afanasiev, J. R. Hortensius, B. A. Ivanov, A. Sasani, E. Bousquet, Y. M. Blanter, R. V. Mikhaylovskiy, A. V. Kimel, and A. D. Caviglia, "Ultrafast control of magnetic interactions via light-driven phonons," Nat. Mater. **20**, 607–611 (2021).

[38] L. C.M. Miranda, "Phonon damping in the simultaneous presence of intense radiation and magnetic fields," J. Phys. C **9**, 2971 (1976).

[39] O. A.C. Nunes, "Carrier-assisted laser pumping of optical phonons in semiconductors under strong magnetic fields," Phys. Rev. B **29**, 5679 (1984).

[40] O. A.C. Nunes, "Amplification of acoustic lattice vibrations by electrons in semiconductors under intense laser radiation," J. Appl. Phys. **56**, 2694 (1984).

[41] A. L. Tronconi and O. A.C. Nunes, "Theory of the excitation and amplification of longitudinal-optical phonons in degenerate semiconductors under an intense laser field," Phys. Rev. B **33**, 4125 (1986).

[42] Eric A. Kittlaus, Heedeuk Shin, and Peter T. Rakich, "Large Brillouin amplification in silicon," Nat. Photonics **10**, 463–467 (2016).

[43] S. M. Komirenko, K. W. Kim, A. A. Demidenko, V. A. Kochelap, and M. A. Stroscio, "Generation and amplification of sub-THz coherent acoustic phonons under the drift of two-dimensional electrons," Phys. Rev. B **62**, 7459 (2000).

[44] Harold N. Spector, "Amplification of Acoustic Waves through Interaction with Conduction Electrons," Phys. Rev. **127**, 1084 (1962).

[45] M. Komirenko, W. Kim, A. Kochelap, V. Koroteev, and A. Stroscio, "Nonlinear regimes of coherent optical phonon generation in quantum wells under electric current pumping," Phys. Rev. B **68**, 155308 (2003).

[46] Keisuke Shinokita, Klaus Reimann, Michael Woerner, Thomas Elsaesser, Rudolf Hey, and Christos Flytzanis, "Strong Amplification of Coherent Acoustic Phonons by Intraminiband Currents in a Semiconductor Superlattice," Phys. Rev. Lett. **116**, 075504 (2016).

[47] S. Wallentowitz, W. Vogel, I. Siemers, and P. E. Toschek, "Vibrational amplification by stimulated emission of radiation," Phys. Rev. A **54**, 943 (1996).

[48] K. Vahala, M. Herrmann, S. Knünz, V. Batteiger, G. Saathoff, T. W. Hänsch, and Th. Udem, "A phonon laser," Nat. Phys. **5**, 682–686 (2009).

[49] Michael Ip, Anthony Ransford, Andrew M. Jayich, Xueping Long, Conrad Roman, and Wesley C. Campbell, "Phonon Lasing from Optical Frequency Comb Illumination of Trapped Ions," Phys. Rev. Lett. **121**, 043201 (2018).

[50] Robert M. Pettit, Wenchao Ge, P. Kumar, Danika R. Luntz-Martin, Justin T. Schultz, Levi P. Neukirch, M. Bhattacharya, and A. Nick Vamivakas, "An optical tweezer phonon laser," Nat. Photonics **13**, 402–405 (2019).

[51] Ivan S. Grudinin, Hansuek Lee, O. Painter, and Kerry J. Vahala, "Phonon laser action in a tunable two-level system," Phys. Rev. Lett. **104**, 083901 (2010).

[52] Hui Jing, S. K. Özdemir, Xin You Lü, Jing Zhang, Lan Yang, and Franco Nori, "PT -symmetric phonon laser," Phys. Rev. Lett. **113**, 053604 (2014).

[53] D. L. Chafatinos, A. S. Kuznetsov, S. Anguiano, A. E. Bruchhausen, A. A. Reynoso, K. Biermann, P. V. Santos, and A. Fainstein, "Polariton-driven phonon laser," Nat. Commun. **11**, 1–8 (2020).

[54] H. Lü, S. K. Özdemir, L. M. Kuang, Franco Nori, and H. Jing, "Exceptional Points in Random-Defect Phonon Lasers," Phys. Rev. Appl. **8**, 044020 (2017).

[55] Guanzhong Wang, Min Xiao, Mingming Zhao, Xiaoshun Jiang, Yingchun Qin, and Zhangqi Yin, "Demonstration of an ultra-low-threshold phonon laser with coupled microtoroid resonators in vacuum," Photonics Res. **5**, 73–76 (2017).

[56] Jing Zhang, Bo Peng, ahin Kaya Özdemir, Kevin Pichler, Dmitry O. Krimer, Guangming Zhao, Franco Nori, Yu xi Liu, Stefan Rotter, and Lan Yang, "A phonon laser operating at an exceptional point," Nat. Photonics **12**, 479–484 (2018).

[57] Igor Bargatin and M. L. Roukes, "Nanomechanical analog of a laser: Amplification of mechanical oscillations by stimulated zeeman transitions," Phys. Rev. Lett. **91**, 138302 (2003).

[58] Ming Song Ding, Li Zheng, and Chong Li, "Phonon laser in a cavity magnomechanical system," Sci. Rep. **9**, 1–8 (2019).

[59] R. P. Beardsley, A. V. Akimov, M. Henini, and

A. J. Kent, "Coherent terahertz sound amplification and spectral line narrowing in a stark ladder superlattice," Phys. Rev. Lett. **104**, 085501 (2010).
[60] A. Cartella, T. F. Nova, M. Fechner, R. Merlin, and A. Cavalleri, "Parametric amplification of optical phonons," Proc. Natl. Acad. Sci. **115**, 12148–12151 (2018).
[61] S. Ghosh, I. Calizo, D. Teweldebrhan, E. P. Pokatilov, D. L. Nika, A. A. Balandin, W. Bao, F. Miao, and C. N. Lau, "Extremely high thermal conductivity of graphene: Prospects for thermal management applications in nanoelectronic circuits," Appl. Phys. Lett. **92**, 151911 (2008).
[62] S. T. Zavtrak and I. V. Volkov, "Sasers (sound amplification by stimulated emission of radiation) in the nonlinear operating regime with various emitters," Tech. Phys. **42**, 793–796 (1997).
[63] Rafi Bistritzer and Allan H. MacDonald, "Moiré bands in twisted double-layer graphene," Proc. Natl. Acad. Sci. **108**, 12233–12237 (2011).
[64] Yuan Cao, Valla Fatemi, Ahmet Demir, Shiang Fang, Spencer L. Tomarken, Jason Y. Luo, Javier D. Sanchez-Yamagishi, Kenji Watanabe, Takashi Taniguchi, Efthimios Kaxiras, Ray C. Ashoori, and Pablo Jarillo-Herrero, "Correlated insulator behaviour at half-filling in magic-angle graphene superlattices," Nature **556**, 80–84 (2018).
[65] Yuan Cao, Valla Fatemi, Shiang Fang, Kenji Watanabe, Takashi Taniguchi, Efthimios Kaxiras, and Pablo Jarillo-Herrero, "Unconventional superconductivity in magic-angle graphene superlattices," Nature **556**, 43–50 (2018).
[66] Pulickel Ajayan, Philip Kim, and Kaustav Banerjee, "Two-dimensional van der Waals materials," Phys. Today **69**, 38 (2016).
[67] Leon Balents, Cory R. Dean, Dmitri K. Efetov, and Andrea F. Young, "Superconductivity and strong correlations in moiré flat bands," Nat. Phys. **16**, 725–733 (2020).
[68] Mikito Koshino and Young-Woo Son, "Moiré phonons in twisted bilayer graphene," Phys. Rev. B **100**, 075416 (2019).
[69] Mikito Koshino and Nguyen N.T. Nam, "Effective continuum model for relaxed twisted bilayer graphene and moiré electron-phonon interaction," Phys. Rev. B **101**, 195425 (2020).
[70] Hiroaki Ishizuka, Ali Fahimniya, Francisco Guinea, and Leonid Levitov, "Purcell-like Enhancement of Electron-Phonon Interactions in Long-Period Superlattices: Linear-Temperature Resistivity and Cooling Power," Nano Lett. **21**, 7465–7471 (2021).
[71] Girish Sharma, Indra Yudhistira, Nilotpal Chakraborty, Derek Y.H. Ho, M. M.Al Ezzi, Michael S. Fuhrer, Giovanni Vignale, and Shaffique Adam, "Carrier transport theory for twisted bilayer graphene in the metallic regime," Nat. Commun. **12**, 1–11 (2021).
[72] Yariv Amnon, *Quantim Electronics* (JOHN WILET & SONS ,INC ., 1988).
[73] We do not consider the flexural modes of suspended graphene.
[74] Otherwise one needs to compute the full electronic steady state in the presence of the tunneling from the leads and relaxation, which we leave for future investigation.
[75] John M.J. Madey, "Stimulated Emission of Bremsstrahlung in a Periodic Magnetic Field," J. Appl. Phys. **42**, 1906 (2003).
[76] C. Pellegrini, A. Marinelli, and S. Reiche, "The physics of x-ray free-electron lasers," Rev. Mod. Phys. **88**, 015006 (2016).
[77] A. Friedman, A. Gover, G. Kurizki, S. Ruschin, and A. Yariv, "Spontaneous and stimulated emission from quasifree electrons," Rev. Mod. Phys. **60**, 471 (1988).
[78] C. W. Roberson and P. Sprangle, "A review of freeelectron lasers," Phys. Fluids B **1**, 3 (1998).
[79] See supplemental material for derivation, which includes Refs. [112, 113].
[80] Eva Y. Andrei and Allan H. MacDonald, "Graphene bilayers with a twist," Nat. Mater. **19**, 1265–1275 (2020).
[81] Mikito Koshino, Noah F.Q. Yuan, Takashi Koretsune, Masayuki Ochi, Kazuhiko Kuroki, and Liang Fu, "Maximally Localized Wannier Orbitals and the Extended Hubbard Model for Twisted Bilayer Graphene," Phys. Rev. X **8**, 031087 (2018).
[82] A spatially modulated perturbation also modifies the electron and phonon dispersions, by opening minigaps at $\pm \boldsymbol{k}_u/2$, which do not affect the phase space region relevant for lasing.
[83] Shikai Deng and Vikas Berry, "Wrinkled, rippled and crumpled graphene: An overview of formation mechanism, electronic properties, and applications," Mater. Today **19**, 197–212 (2016).
[84] Riccardo Frisenda, Matthias Drüppel, Robert Schmidt, Steffen Michaelis de Vasconcellos, David Perez de Lara, Rudolf Bratschitsch, Michael Rohlfing, and Andres Castellanos-Gomez, "Biaxial strain tuning of the optical properties of single-layer transition metal dichalcogenides," npj 2D Mater. Appl. **1**, 1–7 (2017).
[85] U. Ludacka, M. R.A. Monazam, C. Rentenberger, M. Friedrich, U. Stefanelli, J. C. Meyer, and J. Kotakoski, "In situ control of graphene ripples and strain in the electron microscope," npj 2D Mater. Appl. **2**, 1–6 (2018).
[86] Riju Banerjee, Viet Hung Nguyen, Tomotaroh Granzier-Nakajima, Lavish Pabbi, Aurelien Lherbier, Anna Ruth Binion, Jean Christophe Charlier, Mauricio Terrones, and Eric William Hudson, "Strain Modulated Superlattices in Graphene," Nano Lett. **20**, 3113–3121 (2020).
[87] C. C. Hsu, M. L. Teague, J. Q. Wang, and N. C. Yeh, "Nanoscale strain engineering of giant pseudo-magnetic fields, valley polarization, and topological channels in graphene," Sci. Adv. **6** (2020).
[88] Zhen Bi, Noah F.Q. Yuan, and Liang Fu, "Designing flat bands by strain," Phys. Rev. B **100**, 035448 (2019).
[89] Eros Mariani and Felix Von Oppen, "Temperature-dependent resistivity of suspended graphene," Phys. Rev. B **82**, 195403 (2010).
[90] E. H. Hwang and S. Das Sarma, "Dielectric function, screening, and plasmons in two-dimensional graphene," Phys. Rev. B **75**, 205418 (2007).
[91] Felix Von Oppen, Francisco Guinea, and Eros Mariani, "Synthetic electric fields and phonon damping in carbon nanotubes and graphene," Phys. Rev. B **80**, 075420 (2009).
[92] Hidekatsu Suzuura and Tsuneya Ando, "Phonons and electron-phonon scattering in carbon nanotubes," Phys. Rev. B **65**, 235412 (2002).
[93] J. L. Mañes, "Symmetry-based approach to electron-

phonon interactions in graphene," Phys. Rev. B **76**, 045430 (2007).
[94] Thibault Sohier, Matteo Calandra, Cheol Hwan Park, Nicola Bonini, Nicola Marzari, and Francesco Mauri, "Phonon-limited resistivity of graphene by first-principles calculations: Electron-phonon interactions, strain-induced gauge field, and Boltzmann equation," Phys. Rev. B **90**, 125414 (2014).
[95] Cheol Hwan Park, Nicola Bonini, Thibault Sohier, Georgy Samsonidze, Boris Kozinsky, Matteo Calandra, Francesco Mauri, and Nicola Marzari, "Electron-Phonon Interactions and the Intrinsic Electrical Resistivity of Graphene," Nano Lett. **14**, 1113–1119 (2014).
[96] M. Kim, S. G. Xu, A. I. Berdyugin, A. Principi, S. Slizovskiy, N. Xin, P. Kumaravadivel, W. Kuang, M. Hamer, R. Krishna Kumar, R. V. Gorbachev, K. Watanabe, T. Taniguchi, I. V. Grigorieva, V. I. Fal'ko, M. Polini, and A. K. Geim, "Control of electron-electron interaction in graphene by proximity screening," Nat. Commun. **11**, 1–6 (2020).
[97] Nicola Bonini, Jivtesh Garg, and Nicola Marzari, "Acoustic phonon lifetimes and thermal transport in free-standing and strained graphene," Nano Lett. **12**, 2673–2678 (2012).
[98] W. Maryam, A. V. Akimov, R. P. Campion, and A. J. Kent, "Dynamics of a vertical cavity quantum cascade phonon laser structure," Nat. Commun. **4**, 1–6 (2013).
[99] Or Katz, Gil Refael, and Netanel H. Lindner, "Optically induced flat bands in twisted bilayer graphene," Phys. Rev. B **102**, 155123 (2020).
[100] Martin Rodriguez-Vega, Michael Vogl, and Gregory A. Fiete, "Low-frequency and MoiréFloquet engineering: A review," Ann. Phys. (N. Y). **435**, 168434 (2021).
[101] Hannes Hübener, Umberto De Giovannini, and Angel Rubio, "Phonon Driven Floquet Matter," Nano Lett. **18**, 1535–1542 (2018).
[102] W. E. Bron, "Spectroscopy of high-frequency phonons," Reports Prog. Phys. **43**, 301 (1980).
[103] M N Wybournet and J K Wigmore, "Phonon spectroscopy," Reports Prog. Phys. **51**, 923 (1988).
[104] Dominik M. Juraschek and Prineha Narang, "Magnetic control in the terahertz," Science **374**, 1555–1556 (2021).
[105] Zachary A.H. Goodwin, Valerio Vitale, Xia Liang, Arash A. Mostofi, and Johannes Lischner, "Hartree theory calculations of quasiparticle properties in twisted bilayer graphene," Electron. Struct. **2**, 034001 (2020).
[106] Hoi Chun Po, Liujun Zou, Ashvin Vishwanath, and T. Senthil, "Origin of Mott Insulating Behavior and Superconductivity in Twisted Bilayer Graphene," Phys. Rev. X **8**, 031089 (2018).
[107] Nick Bultinck, Eslam Khalaf, Shang Liu, Shubhayu Chatterjee, Ashvin Vishwanath, and Michael P. Zaletel, "Ground State and Hidden Symmetry of Magic-Angle Graphene at even Integer Filling," Phys. Rev. X **10**, 031034 (2020).
[108] Y. H. Kwan, G. Wagner, T. Soejima, M. P. Zaletel, S. H. Simon, S. A. Parameswaran, and N. Bultinck, "Kekulé Spiral Order at All Nonzero Integer Fillings in Twisted Bilayer Graphene," Phys. Rev. X **11**, 041063 (2021).
[109] Glenn Wagner, Yves H. Kwan, Nick Bultinck, Steven H. Simon, and S. A. Parameswaran, "Global Phase Diagram of the Normal State of Twisted Bilayer Graphene," Phys. Rev. Lett. **128**, 156401 (2022).
[110] Fabrizio Illuminati and Alexander Albus, "High-temperature atomic superfluidity in lattice Bose-Fermi mixtures," Phys. Rev. Lett. **93**, 090406 (2004).
[111] D. W. Wang, M. D. Lukin, and E. Demler, "Engineering superfluidity in Bose-Fermi mixtures of ultracold atoms," Phys. Rev. A **72**, 051604 (2005).
[112] D. Svintsov, V. Vyurkov, S. Yurchenko, T. Otsuji, and V. Ryzhii, "Hydrodynamic model for electron-hole plasma in graphene," J. Appl. Phys. **111**, 083715 (2012).
[113] Loïc Huder, Alexandre Artaud, Toai Le Quang, Guy Trambly De Laissardière, Aloysius G.M. Jansen, Gérard Lapertot, Claude Chapelier, and Vincent T. Renard, "Electronic Spectrum of Twisted Graphene Layers under Heterostrain," Phys. Rev. Lett. **120**, 156405 (2018).